

Multi-symplectic discretisation of wave map equations

David Cohen^{*1} and Olivier Verdier^{†1}

¹*Department of Mathematics and Mathematical Statistics, Umeå University, Sweden*

2024-12-07

A new multi-symplectic formulation of constrained Hamiltonian partial differential equations is presented, and the associated local conservation laws are studied. A multi-symplectic discretisation based on this new formulation is exemplified by means of the Euler box scheme. When applied to the wave map equation, this numerical scheme is explicit, preserves the constraint and can be seen as a direct generalisation of the SHAKE algorithm for constrained mechanical systems. Furthermore, numerical experiments show excellent conservation properties of the numerical solutions.

Keywords Constrained Hamiltonian partial differential equations · Wave map equations · Multi-symplectic partial differential equation · Numerical discretisation · Multi-symplectic schemes · Euler box scheme

Mathematics Subject Classification (2010) 35Q51 · 35Q53 · 37K05 · 37K10 · 37M15 · 65M06 · 65M99 · 65P10

1 Introduction

The interest for multi-symplectic discretisation techniques may be measured by noting that the seminal papers on this subject [18] and [8], have acquired well over seven hundred citations on Google Scholar. One purpose of this article is thus to extend the notion of Hamiltonian partial differential equations (PDEs) with a multi-symplectic structure, see for example [7, 8, 17], to Hamiltonian PDEs subject to constraints. Based on this structure, a multi-symplectic numerical integrator is then derived.

^{*}david.cohen@math.umu.se

[†]olivier.verdier@math.umu.se

In order to illustrate the main properties of this new multi-symplectic numerical method for Hamiltonian PDEs with constraints, we will focus our numerical analysis on the discretisation of wave map equations on the sphere (or on the circle)

$$\begin{aligned} u_{tt}(x, t) - \Delta u(x, t) &= \lambda u(x, t) \quad \text{in } \Omega \times (0, \infty) \\ |u(x, t)| &= 1 \\ u(x, 0) &= u_0(x), \quad u_t(x, 0) = v_0(x), \end{aligned}$$

where the “domain” $\Omega \subset \mathbb{R}^m$ is an m -dimensional box or torus, $u \in \mathbb{S}^\ell$ for the “target” manifold \mathbb{S}^2 (the sphere) or \mathbb{S}^1 (the circle), and λ is a Lagrange multiplier. Here, the initial position u_0 and velocity v_0 (living in the tangent space of the target manifold) of the wave are given. This nonlinear PDE has applications in general relativity and in particle physics, see [25, 23, 31, 2] and references therein for details. The above wave map equation has received considerable attention, from a more theoretical point of view, during the last decades. This equation is integrable; has a conserved energy; is time reversible; is non dissipative; is invariant with respect to the scaling $u(x, t) \rightarrow u(\lambda x, \lambda t)$ for $\lambda \in \mathbb{R}$; is related to Einstein equations; is related to the sine-Gordon equation; has critical regularity $m/2$; possesses, for example, global smooth solutions if the initial data are smooth and if the domain is \mathbb{R}^1 ; has blow-up solutions in finite time if the domain is \mathbb{R}^m with $m \geq 3$; it is however an open problem to show if smooth solutions do become singular in finite time; etc. [22, 5, 28, 25, 15, 29, 30, 26, 27, 31, 32, 16]

The literature on the numerical analysis of the wave map equation is, on the other hand, relatively scarce. The earlier references [6, 13] report numerical evidences of finite-time blow-up of smooth initial data. These works restrict to equivariant maps, where the wave map equation reduces to a semilinear scalar wave equation. This scalar problem is then discretised with the standard leapfrog scheme or the Crank–Nicholson scheme with adaptive mesh. Very recently, there has been a renewed interest for the numerical discretisation of wave map problems starting with the series of papers [3, 2, 4, 1]. These works prove convergence of certain (semi)-implicit finite element based methods to weak solutions of wave map equations. The main aim of reference [21] is to compare the evolution of (the blow-up of) equivariant maps using the classical Runge–Kutta 4 scheme and the RATTLE algorithm for the time discretisation of wave map equations. Here, the authors used the method of lines to discretise the PDE and a five-point formulae for the spatial derivatives. Our multi-symplectic numerical methods shares similarities with the RATTLE algorithm (as we shall see in § 3 that it is the SHAKE algorithm in time, and RATTLE is almost identical to SHAKE [19, § 5.1.2]) but we would like to point out that our formalism is more general than the one proposed in [21]. In addition, the authors of the previously cited paper analyse, for the first time, the blow-up dynamics and singularity formation in the nonequivariant case using the same numerical methods in reference [9]. Furthermore, the recent publication [14] presents a finite difference method applied to a reformulation of the wave map equation. The proposed method conserves the energy, the constraint and converges to the weak solution of the wave map equation. This numerical method is however nonlinear and implicit.

In the present article, we will derive and study a multi-symplectic numerical integrator

for the above wave map equation. This scheme takes the particular simple form

$$\frac{u^{n,i+1} - 2u^{n,i} + u^{n,i-1}}{\Delta t^2} - \frac{u^{n+1,i} - 2u^{n,i} + u^{n-1,i}}{\Delta x^2} = -\lambda u^{n,i}$$

$$|u^{n,i+1}| = 1,$$

where $u^{n,i} \approx u(x_n, t_i)$ on a uniform rectangular grid with meshes Δx and Δt . The proposed numerical scheme is explicit (because λ is determined explicitly by (13)), conserves the multi-symplectic structure of the wave map equation, preserves the constraint and can be seen as a direct generalisation of the SHAKE algorithm for constrained mechanical systems [12, Sect. VII.1.4] [19], to Hamiltonian PDEs with constraints. All these features will be analysed in the rest of the paper which is organised as follows. Section 2 presents new multi-symplectic formulation and discretisation of general Hamiltonian PDEs with constraint. This is then illustrate for the particular case of wave map equations in Section 3. The paper ends with concluding remarks in Section 4.

2 Multi-symplectic Hamiltonian PDEs with constraint

In this section, we consider the numerical discretisation of partial differential equations subject to a constraint

$$F(x_1, x_2, \dots, x_m, t, u, \frac{\partial u}{\partial x_1}, \dots, \frac{\partial u}{\partial t}, \dots) = 0$$

$$g(u) = 0,$$

where $u(x_1, x_2, \dots, x_m, t) \in \mathbb{R}^\ell$ and $g: \mathbb{R}^\ell \rightarrow \mathbb{R}$. More precisely, we will begin this section by extending the concept of multi-symplectic PDEs to multi-symplectic PDEs with constraint. We will then use this new multi-symplectic formulation to derive a multi-symplectic numerical scheme for the above type of problems.

2.1 Multi-symplectic formulation of the equations

There are two standard ways to construct multi-symplectic formulations of a PDE. One approach is using the Lagrangian formulation of the problem, see the early references [11, 18] and references therein. The other approach is to write the partial differential equation as a system of equations containing only first-order derivatives in space and time, see equation (1) below, and then to extract the multi-symplectic structure, see the early references [7, 8, 17] and references therein.

We will now generalise this second approach to PDE with constraints. To do this, let $n \geq 3$, two skew-symmetric matrices $M, K \in \mathbb{R}^{n \times n}$ and a scalar function $S: \mathbb{R}^n \rightarrow \mathbb{R}$.

We consider *Hamiltonian systems on a multi-symplectic structure with constraint*

$$Mz_t + Kz_x = \nabla_z S(z) - \begin{pmatrix} \lambda \nabla g(z_1) \\ 0 \\ \vdots \\ 0 \end{pmatrix}$$

$$g(z_1) = 0. \quad (1)$$

Here, $z = z(x, t) \in \mathbb{R}^n$ is the state variable with components $z = (z_1, \dots, z_n)$ with $z_1 := u$. λ is a Lagrange multiplier, $x \in [0, 1]$ (for simplicity, see the remark below) and $t > 0$. The motion is thus constrained to satisfy $g(z_1) = 0$, where $g: \mathbb{R}^\ell \rightarrow \mathbb{R}$ and $\nabla g(z_1)$ denotes the gradient of g .

Remark 2.1. The above definition can be generalised to higher dimensions. Indeed, if one wants to consider $u = (u_1, u_2, u_3) \in \mathbb{R}^3$ (or any higher dimension), one sets $z_1 := (u_1, u_2, u_3)$. In a similar way, one can further treat the case $x = (x_1, x_2) \in [0, 1]^2$ (or any higher dimension) considering the multi-symplectic formulation

$$Mz_t + K_1 z_{x_1} + K_2 z_{x_2} = \nabla_z S(z) - \begin{pmatrix} \lambda \nabla g(z_1) \\ 0 \\ \vdots \\ 0 \end{pmatrix}$$

$$g(z_1) = 0$$

with three skew-symmetric matrices M, K_1 and K_2 .

2.2 Conservation laws

From the formulation (1), we shall now introduce the conservation laws (CL) of multi-symplecticity, energy and momentum. These derivations follow the lines of [17, Chap. 12]. Let us first consider the variational equation of (1)

$$Md z_t + K d z_x = S_{zz}(z) d z - \begin{pmatrix} d(\lambda \nabla g(z_1)) \\ 0 \\ \vdots \\ 0 \end{pmatrix}$$

$$\nabla g(z_1) d z_1 = 0.$$

Taking the wedge product of the above expression with $d z$, using the symmetry of $S_{zz}(z)$ and $G'(z)$, and using the constraint, one then obtains the *CL of multi-symplecticity*

$$\omega_t + \kappa_x = 0 \quad (2)$$

with

$$\omega := \frac{1}{2} d z \wedge M d z \quad \text{and} \quad \kappa := \frac{1}{2} d z \wedge K d z.$$

As noted in [20], this CL of multi-symplecticity can be simplified by taking a non-unique splitting of the matrices M and K (see also Subsection 2.3 below) such that

$$M = M_+ + M_-, \quad K = K_+ + K_-,$$

where

$$M_+^T = -M_- \quad \text{and} \quad K_+^T = -K_-.$$

Hence (2) holds with

$$\omega = dz \wedge M_+ dz \quad \text{and} \quad \kappa = dz \wedge K_+ dz.$$

One next obtains the CL of energy by taking the usual scalar product (denoted by $\langle \cdot, \cdot \rangle$) of (1) with z_t . Notting that $\langle z_t, M z_t \rangle = 0$, one gets

$$\langle z_t, K_+ z_x + K_- z_x \rangle = \langle z_t, \nabla_z S(z) \rangle - \langle z_t, \begin{pmatrix} (\lambda \nabla g(z_1)) \\ 0 \\ \vdots \\ 0 \end{pmatrix} \rangle.$$

Since $\langle z_t, K_+ z_x + K_- z_x \rangle = \partial_x (\langle z_t, K_+ z \rangle) - \partial_t (\langle z_x, K_+ z \rangle)$ and $\langle z_t, \nabla_z S(z) \rangle = \partial_t (\nabla_z S(z))$, one obtains the *CL of energy*

$$E_t(z) + F_x(z) = 0 \tag{3}$$

with the density functions

$$\begin{aligned} E(z) &= S(z) + \langle z_x, K_+ z \rangle \\ F(z) &= -\langle z_t, K_+ z \rangle. \end{aligned}$$

Similarly, the *CL of momentum* reads

$$I_t(z) + J_x(z) = 0 \tag{4}$$

with the density functions

$$\begin{aligned} I(z) &= -\langle z_x, M_+ z \rangle \\ J(z) &= S(z) + \langle z_t, M_+ z \rangle. \end{aligned}$$

2.3 Multi-symplectic discretisation of Hamiltonian PDEs with constraint

The goal of this subsection is now to construct a numerical method for (1) which preserves a discrete analog of the conservation law of multi-symplecticity (2).

To do this, we first extend the Euler box scheme, see for example [20], to constrained Hamiltonian PDE (1). We set $\Delta x = x_{n+1} - x_n, n \in \mathbb{N}$, and $\Delta t = t_{i+1} - t_i, i \geq 0$. Moreover, we define the forward and backward differences in time

$$\delta_t^+ z^{n,i} = \frac{z^{n,i+1} - z^{n,i}}{\Delta t} \quad \text{and} \quad \delta_t^- z^{n,i} = \frac{z^{n,i} - z^{n,i-1}}{\Delta t},$$

and similarly for differences in space.

Further, we introduce a splitting of the two matrices M and K in (1), setting $M = M_+ + M_-$, $K = K_+ + K_-$ where $M_+^T = -M_-$ and $K_+^T = -K_-$. In this article, we will only consider this particular splitting, keeping in mind that the above splitting of the matrices is not unique. We now apply the symplectic Euler method to the temporal and spatial discretisation of (1). This gives us the *Euler box scheme for constrained Hamiltonian PDE* (1)

$$M_+ \delta_t^+ z^{n,i} + M_- \delta_t^- z^{n,i} + K_+ \delta_x^+ z^{n,i} + K_- \delta_x^- z^{n,i} = \nabla_z S(z^{n,i}) - \lambda \begin{pmatrix} \nabla g(z_1^{n,i}) \\ 0 \\ \vdots \\ 0 \end{pmatrix}$$

$$g(z_1^{n+1,i}) = 0, \quad (5)$$

where $z^{n,i} \approx z(x_n, t_i)$ on a uniform rectangular grid.

To conclude this subsection, we show that the Euler box scheme (5) is a multi-symplectic integrator.

Proposition 2.2. *We consider the Euler box scheme (5) with $M_+^T = -M_-$ and $K_+^T = -K_-$. The Euler box scheme (5) for constrained Hamiltonian PDE (1) satisfies the following discrete multi-symplectic conservation law*

$$\delta_t^+(dz^{n,i-1} \wedge M_+ dz^{n,i}) + \delta_x^+(dz^{n-1,i} \wedge K_+ dz^{n,i}) = 0. \quad (6)$$

In analogy to the original definition of multi-symplectic integrators from [8], we thus call this numerical method a multi-symplectic integrator for (1).

Proof. The proof follows the lines of the proof of [20, Prop. 1]. We start the proof by considering the discrete variational equation

$$M_+ \delta_t^+ dz^{n,i} + M_- \delta_t^- dz^{n,i} + K_+ \delta_x^+ dz^{n,i} + K_- \delta_x^- dz^{n,i} = S_{zz}(z^{n,i}) dz^{n,i} - d \begin{pmatrix} \lambda \nabla g(z_1^{n,i}) \\ 0 \\ \vdots \\ 0 \end{pmatrix}$$

$$\nabla g(z_1^{n,i}) dz^{n,i} = 0.$$

Taking the wedge product of the above expression with $dz^{n,i}$, we obtain

$$dz^{n,i} \wedge \left(M_+ \delta_t^+ dz^{n,i} + M_- \delta_t^- dz^{n,i} \right) + dz^{n,i} \wedge \left(K_+ \delta_x^+ dz^{n,i} + K_- \delta_x^- dz^{n,i} \right) =$$

$$dz^{n,i} \wedge S_{zz}(z^{n,i}) dz^{n,i} - \begin{pmatrix} dz_1^{n,i} \wedge (d\lambda \nabla g(z_1^{n,i})) + dz_1^{n,i} \wedge G'(z_1^{n,i}) dz_1^{n,i} \lambda \\ 0 \\ \vdots \\ 0 \end{pmatrix}.$$

Using properties of the wedge product, the symmetry of $S_{zz}(z)$ and $G'(z)$, and the fact that the numerical solution given by (5) satisfies the constraint, we end up with the discrete conservation law (6). \square

3 Applications to wave map equations

In this section, we show that the wave map equation possesses a multi-symplectic formulation. Furthermore, we derive an Euler box scheme for the wave map equation and show that this multi-symplectic numerical method has a particular simple form which is closely related to the SHAKE algorithm. Finally, we perform numerical experiments in order to illustrate the main properties of the numerical solutions.

3.1 A multi-symplectic formulation of wave map equations

Wave map problems with a smooth potential V [27, 10, 34]

$$\begin{aligned} u_{tt} - u_{xx} &= -V'(u) + \lambda \nabla g(u) \\ g(u) &= 0, \end{aligned} \tag{7}$$

where $u = (u_1, u_2, u_3) \in \mathbb{R}^3$, can be put into the multi-symplectic framework (1). For ease of presentation, we will only consider a domain in \mathbb{R}^1 here. An example on a 2-dimensional torus will be given in Subsection 3.3.

Indeed, considering the vector of state variable $z = (u_1, u_2, u_3, v_1, v_2, v_3, m_1, m_2, m_3)$, taking the skew-symmetric matrices (I denotes the identity matrix in \mathbb{R}^3)

$$M = \begin{pmatrix} 0 & -I & 0 \\ I & 0 & 0 \\ 0 & 0 & 0 \end{pmatrix} \quad \text{and} \quad K = \begin{pmatrix} 0 & 0 & -I \\ 0 & 0 & 0 \\ I & 0 & 0 \end{pmatrix}$$

and considering the scalar function $S(z) = \frac{1}{2}(v_1, v_2, v_3)^T(v_1, v_2, v_3) - \frac{1}{2}(m_1, m_2, m_3)^T(m_1, m_2, m_3) + V(u_1, u_2, u_3)$ we obtain the equivalent representation (1) with $z_1 = (u_1, u_2, u_3)$. This multi-symplectic formulation of the wave map equation (7) takes the explicit form

$$\begin{aligned} -v_t - m_x &= V'(u) - \lambda \nabla g(u) \\ u_t &= v \\ u_x &= -m \\ g(u) &= 0. \end{aligned}$$

In particular, taking $V \equiv 0$ and $g(u) = |u| - 1$ in (7), one gets a multi-symplectic formulation (1) of the classical wave map problem into the unit sphere [28]

$$\begin{aligned} u_{tt} - u_{xx} &= \lambda u \\ |u| &= 1. \end{aligned} \tag{8}$$

For the above wave map problems (7), one may take the splitting of the matrices using

$$M_+ = \begin{pmatrix} 0 & -I & 0 \\ 0 & 0 & 0 \\ 0 & 0 & 0 \end{pmatrix} \quad \text{and} \quad K_+ = \begin{pmatrix} 0 & 0 & -I \\ 0 & 0 & 0 \\ 0 & 0 & 0 \end{pmatrix}.$$

The CL of multi-symplecticness, energy and momentum then read

$$\begin{aligned}
& (du \wedge dv)_t + (du \wedge dm)_x = 0 \\
& \left(\frac{1}{2}v^T v - \frac{1}{2}m^T m + V(u) - (m_x)^T m\right)_t + ((u_t)^T m)_x = 0 \\
& ((u_x)^T v)_t + \left(\frac{1}{2}v^T v - \frac{1}{2}m^T m + V(u) - (u_t)^T v\right)_x = 0.
\end{aligned} \tag{9}$$

Integrating these two last CLs over the spatial domain and using appropriate boundary conditions, one obtains two conserved quantities. Wave map problems (7) are thus Hamiltonian PDEs with constraint and having the following conserved quantities, see also [31, 3],

$$H(u) = \int_{\Omega} \left(\frac{1}{2}|u_t|^2 + \frac{1}{2}|u_x|^2 + V(u)\right) dx \tag{10}$$

$$M(u) = \int_{\Omega} \frac{1}{2}(u_x)^T u_t dx. \tag{11}$$

3.2 A multi-symplectic scheme for wave map equations

For the particular case of wave map problems (7), one can eliminate all the additional variables in the Euler box scheme (5) and express the numerical scheme only in terms of $z_1 = u$. This gives us the following multi-symplectic integrator for wave map equations (7)

$$\begin{aligned}
\delta_t^+ \delta_t^- u^{n,i} - \delta_x^+ \delta_x^- u^{n,i} &= -V'(u^{n,i}) - \lambda \nabla g(u^{n,i}) \\
g(u^{n,i+1}) &= 0.
\end{aligned}$$

Developing all the above terms, the Euler box scheme for wave map equations (7) thus reads

$$\begin{aligned}
\frac{u^{n,i+1} - 2u^{n,i} + u^{n,i-1}}{\Delta t^2} - \frac{u^{n+1,i} - 2u^{n,i} + u^{n-1,i}}{\Delta x^2} &= -V'(u^{n,i}) - \lambda \nabla g(u^{n,i}) \\
g(u^{n,i+1}) &= 0.
\end{aligned} \tag{12}$$

In the wave map case, the constraint manifold is a sphere of radius one. The value of the Lagrange multiplier λ is thus a solution of a quadratic problem. Assuming that u^0 (the first step of the scheme) lies on the sphere of radius one. One then compute a point \widetilde{u}^1 by ignoring the constraint, see Figure 1. We then straightforwardly obtain

$$\lambda = -s + \sqrt{s - \|\widetilde{u}^1\|^2 + 1}, \tag{13}$$

where s is the scalar product $s = \langle u^0, \widetilde{u}^1 \rangle$. As a result, this projection step is an explicit operation.

The above numerical integrator can also be seen as a direct application of the SHAKE algorithm for constrained mechanical systems, see e.g. [19] or [12, Sect. VII.1.4], to wave map equations.

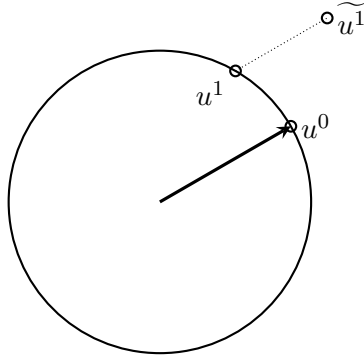


Figure 1: The point u^1 is obtained by first computing a point $\widetilde{u^1}$ by ignoring the constraint. We then project the point $\widetilde{u^1}$ *along the direction of u^0* , to obtain a point u^1 which fulfills the constraints. This means that we have $u^1 = \widetilde{u^1} + \lambda u^0$ for some scalar λ . In the case of a quadratic constraint, the expression for λ is explicit, see (13).

3.3 Numerical experiments

This subsection illustrates the main properties of the Euler box scheme (12) when applied to the wave map equations (7) and (8).

3.3.1 Convergence rates and approximate energy conservation for the wave map on the circle

We consider the wave map problem (8) in two spatial dimensions [14]

$$\begin{aligned} u_{tt} - u_{x_1 x_1} - u_{x_2 x_2} &= \lambda u \\ |u|^2 - 1 &= 0, \end{aligned} \tag{14}$$

where $u = u(x_1, x_2, t) \in \mathbb{R}^2$, with $(x_1, x_2) \in \mathbb{T}^2$ the 2-dimensional torus.

For sake of completeness let us first state the multi-symplectic formulation and the scheme in the present setting. The above wave map problem has the following multi-symplectic formulation

$$\begin{aligned} Mz_t + K_1 z_{x_1} + K_2 z_{x_2} &= \nabla_z S(z) - \begin{pmatrix} \lambda \nabla g(z_1) \\ 0 \\ \vdots \\ 0 \end{pmatrix} \\ g(z_1) &= 0 \end{aligned}$$

with the state variable $z = (u, v, m, p)$, the function $S(z) = \frac{1}{2}v^T v - \frac{1}{2}m^T m - \frac{1}{2}p^T p$, the

Wavenumber	Amplitude	Phase
(1, 1)	1	0
(2, 1)	0.5	0.5
(-1, 1)	0.2	0.8

Table 1: The values of the wavenumbers (pairs of integers), as well as amplitudes (scalar) and phase shifts (angle) used in Figure 2.

constraint $g(u) = |u|^2 - 1$ and the three skew-symmetric matrices

$$M = \begin{pmatrix} 0 & -I & 0 & 0 \\ I & 0 & 0 & 0 \\ 0 & 0 & 0 & 0 \\ 0 & 0 & 0 & 0 \end{pmatrix} \quad \text{and} \quad K_1 = \begin{pmatrix} 0 & 0 & -I & 0 \\ 0 & 0 & 0 & 0 \\ I & 0 & 0 & 0 \\ 0 & 0 & 0 & 0 \end{pmatrix} \quad \text{and} \quad K_2 = \begin{pmatrix} 0 & 0 & 0 & -I \\ 0 & 0 & 0 & 0 \\ 0 & 0 & 0 & 0 \\ I & 0 & 0 & 0 \end{pmatrix}.$$

The corresponding multi-symplectic Euler box scheme, for the classical splitting of the matrices, reads

$$\begin{aligned} \delta_t^+ \delta_t^- u^{n,m,i} - \delta_{x_1}^+ \delta_{x_1}^- u^{n,m,i} - \delta_{x_2}^+ \delta_{x_2}^- u^{n,m,i} &= -\lambda \nabla g(u^{n,m,i}) \\ g(u^{n,m,i+1}) &= 0. \end{aligned} \tag{15}$$

Problem (14) has the following analytical solution:

$$u(x, t) = \left(\cos(\theta(x, t)), \sin(\theta(x, t)) \right) \tag{16}$$

where $x = (x_1, x_2)$ and θ is a solution of the *linear* wave equation

$$\theta_{tt} - \Delta \theta = 0. \tag{17}$$

Such solutions are superpositions of the functions

$$\theta_k(x, t) := a_k \cos(k_1 x_1 + k_2 x_2 - \|k\|t - \varphi_k), \tag{18}$$

where $k = (k_1, k_2) \in \mathbb{Z}^2$ is the *wavenumber*, $a_k \in \mathbb{R}$ is the amplitude, and $\varphi_k \in \mathbb{T}$ is an arbitrary phase shift.

In the following numerical experiments, we thus compute the exact solution of our wave map problem (14) using formulas (16) and (18) and choosing the values a_k , φ_k from Table 1.

We now use our multi-symplectic numerical method (15). Figure 2 shows a plot of the error, i.e., the norm of the difference between the computed solution and the exact solution. The norm used is that of the space $L^\infty(0, T; L^2(\mathbb{T}^2))$, where \mathbb{T}^2 is the spatial domain, the two-dimensional torus. The integer N denotes the number of points in space. The final time is $T = 1$. The Courant Number is chosen at $1/2$, i.e., there are twice as many time points than space points. The slope is 2.15 which indicates convergence of order two.

Figure 3 displays the energy along the numerical solution given by the multi-symplectic scheme (15) on the time interval $[0, 11]$ with $N = 2^7$ points in space. We observe good approximate energy conservation.

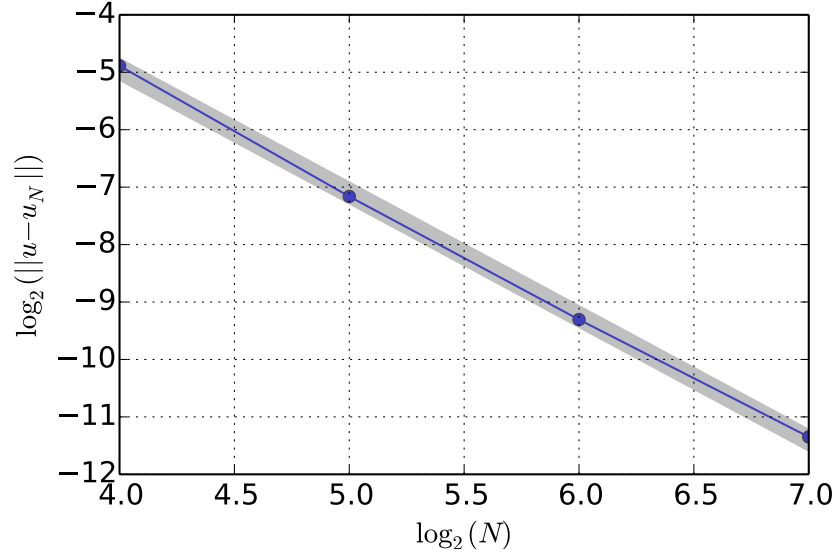


Figure 2: Wave map on the torus: Plot of the error of the computed solution with respect to the exact one. The integer N denotes the number of points in space. The slope is 2.15 which indicates convergence of order two.

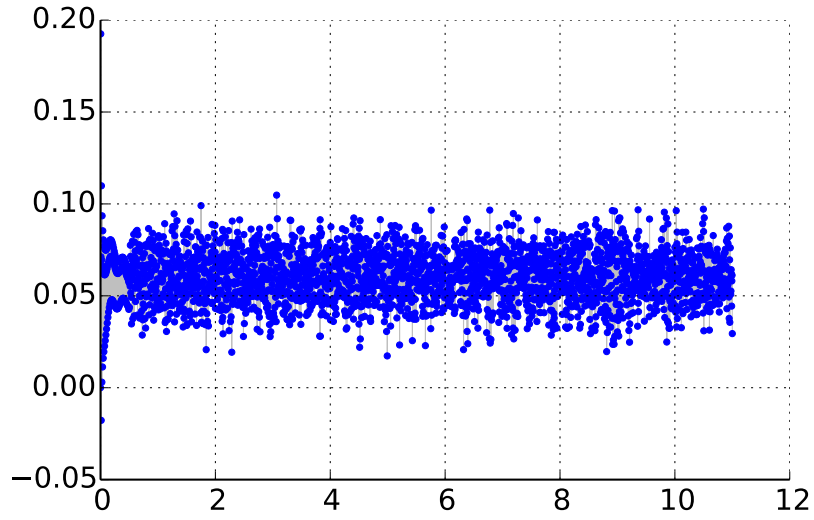


Figure 3: Wave map on the torus: Energy along the numerical solution on the time interval $[0, 11]$.

3.3.2 Breather solutions

We now consider breather solutions of the wave map equation

$$\begin{aligned} u_{tt} - u_{xx} &= \lambda u \\ |u| &= 1, \end{aligned}$$

where $u: \mathbb{R} \times \mathbb{R} \rightarrow \mathbb{R}^3$. We consider the following initial condition

$$u_0 = \begin{pmatrix} \cos(\ell x) \\ \sin(\ell x) \\ 0 \end{pmatrix} \quad (19a)$$

$$u_1 = u_0 + \begin{pmatrix} 0 \\ 0 \\ \varepsilon \sin(jx) \end{pmatrix}, \quad (19b)$$

where ℓ and j are integers such that $1 \leq j \leq \ell - 1$, and ε is an arbitrary small parameter. Observe that the period of the breather wave map tends to infinity when ε goes to zero.

Let us first show that this initial condition is a first order approximation of the breather wave map given by [24, Lemma 7.2]. Indeed, this breather wave map is given by

$$u_b(x, s) := \begin{pmatrix} \cos(\kappa) \cos(\ell x - \kappa) - \sin(\kappa) \cos(s/\sin(\kappa)) \sin(\ell x - \kappa) \\ \cos(\kappa) \sin(\ell x - \kappa) + \sin(\kappa) \cos(s/\sin(\kappa)) \cos(\ell x - \kappa) \\ \sin(\kappa) \sin(s/\sin(\kappa)) \end{pmatrix},$$

where

$$\tan(\kappa) = \frac{\ell}{j} \tan(jx) \quad \text{and} \quad s(x, t) := \int_{-\infty}^t \ell \sin(\alpha(\tau, x)/2) d\tau$$

and

$$\alpha = \alpha(x, t) = 4 \arctan\left(\frac{\sqrt{\ell^2 - j^2}}{j} \frac{\sin(jx)}{\cosh(\sqrt{\ell^2 - j^2}t)}\right)$$

is the classical breather solution of the generalised sine-Gordon equation $\alpha_{tt} - \alpha_{xx} - \ell^2 \sin(\alpha) = 0$.

In fact, the initial condition (19) is obtained using a first order approximation of $u_b(x, s)$ at $s = 0$. First, as noted in [24], using the identity for the sum of angles of trigonometric functions, the value of $u_b(x, 0)$ simply reduces to (19a).

Now, for $t \simeq -\infty$, we have $\cosh(\sqrt{\ell^2 - j^2}t) \simeq \infty$, so we approximate $\alpha(x, t)$ by

$$\alpha(x, t) \simeq 4 \frac{\sqrt{\ell^2 - j^2}}{j} \exp(\sqrt{\ell^2 - j^2}t) \sin(jx).$$

This gives in turn

$$s(x, t) \simeq \int_{-\infty}^t \frac{\ell}{2} \alpha(x, \tau) d\tau$$

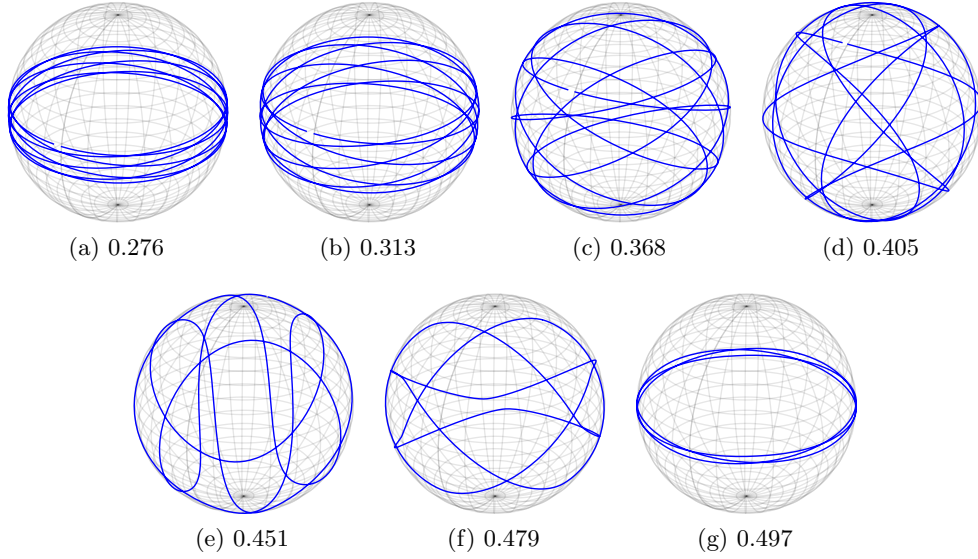


Figure 4: Wave map on \mathbb{R} : Snapshots of the breather of winding number $\ell = 7$ and initial frequency $j = 2$. The caption below each snapshot indicates the time in period units.

so we obtain

$$s(x, t) \simeq 2 \frac{\ell}{j} \exp(\sqrt{\ell^2 - j^2} t) \sin(jx),$$

and we choose

$$\varepsilon := 2 \frac{\ell}{j} \exp(\sqrt{\ell^2 - j^2} t),$$

which is infinitesimally small when $t \simeq -\infty$.

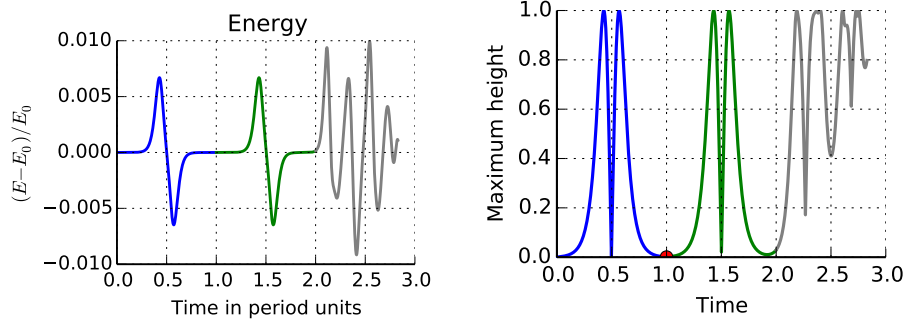
Finally, a first order development of u_b at $s = 0$ yields

$$u_b(x, s) \simeq u_b(x, 0) + \begin{pmatrix} 0 \\ 0 \\ s \end{pmatrix}$$

which justifies the choice (19b).

We now run our multi-symplectic scheme (12) on the example corresponding to the winding number $\ell = 7$ and the initial frequency $j = 2$. The value of ε in (19b) is set to 10^{-5} . Figure 4 presents snapshots of the numerical solutions computed with $N = 2^9$ points in space, and a Courant ratio $\Delta t / \Delta x = 1/2$. We observe a periodic motion, which leads us to define a *period* as the first time at which the numerical solution returns to its initial state. After two periods, the periodic behaviour quickly deteriorates, as shown in Figure 5.

Still using the same data as in the previous numerical experiments, Figure 5 displays the energy and amplitude in the z direction of the numerical solution over three periods.



(a) Plot of the energy E , normalised with the initial energy $E_0 = 967$ (b) Plot of the maximum amplitude in the direction orthogonal to the initial circle

Figure 5: Wave map on \mathbb{R} : Plots of the energy and amplitude in the z direction over three periods. Each period is plotted with a different colour.

These plots, in period units, show that the breathers are not stable. However, it is still a major merit of the proposed numerical method to still compute the first period of the breather fairly accurately.

Finally, Figure 6 shows the energy of the above breather over thirty period units. We use the same colours as in Figure 5. The initial energy is still $E_0 = 967$, so we see that the energy oscillations are minimal, and that there is no energy drift.

3.3.3 Blow-up of smooth initial data

The next numerical experiment deal with the wave map equation

$$\begin{aligned} u_{tt} - \Delta u &= \lambda u \\ |u| &= 1, \end{aligned}$$

where $u = u(x, t) \in \mathbb{R}^3$, $x = (x_1, x_2) \in [-1/2, 1/2]^2$. This problem is supplemented with homogeneous Neumann boundary conditions. We consider the initial data [3, 14]

$$u_0(x_1, x_2) = \frac{1}{a(r)^2 + r^2} \left(2x_1 a(r), 2x_2 a(r), a(r)^2 - r^2 \right) \quad (20)$$

with $r = \sqrt{x_1^2 + x_2^2}$ and

$$a(r) = \begin{cases} (1 - 2r)^4 & r \leq 1/2 \\ 0 & r \geq 1/2. \end{cases}$$

We use our multi-symplectic scheme with $N = 128$ points in each directions in space. Our results are shown in Figure 7 and Figure 8. Looking at the two subplots of Figure 7, we can estimate the blow-up time at 0.28 by glancing at the maximum value of the computed energy. This corresponds to the time where the center particle brutally flips

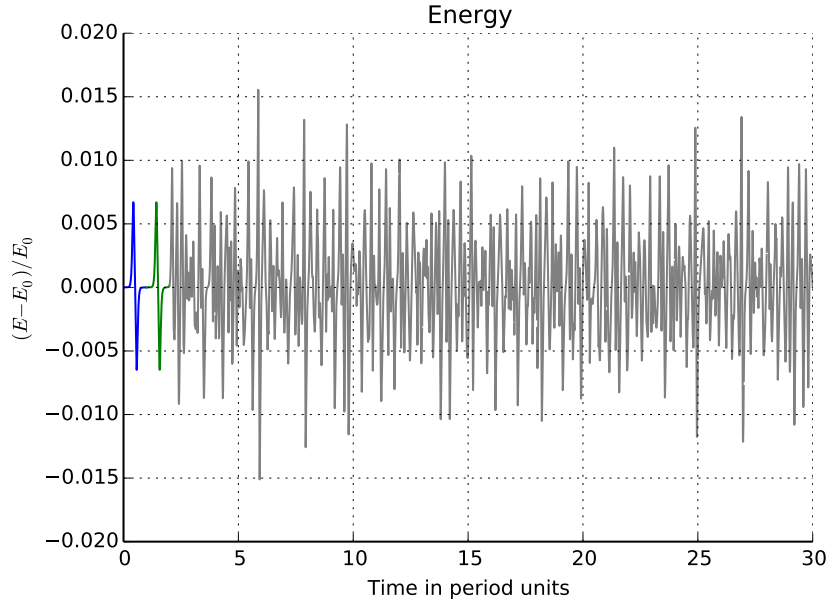


Figure 6: Wave map on \mathbb{R} : Plot of the energy E of the breather of Figure 5 over thirty period units.

over to pointing to the opposite direction $z = -1$. Figure 8 offers a view of the z coordinate versus a radius

These results are in accordance with the numerical experiments done in [3, 14]. In particular, the blow-up time measured in Figure 7a at 0.28, as well as the flip observed in Figure 7b are identical to the ones observed in [3, 14].

3.3.4 Wave map equations with smooth potential

Finally, we consider the discretisation of a wave map equation with the smooth potential

$$V(u) = 400(u_1^2 + u_2^2). \quad (21)$$

The setting is otherwise the same as in §3.3.2. We plot some snapshots of the numerical solution given by our multi-symplectic integrator in Figure 9. The initial condition is a single winding around a big circle of the sphere, tilted from the equator plane at an angle of 45 degrees. It is thus a fixed point of the wave map without potential. That initial condition is not a fixed point of the wave map with potential, as is evidenced by the snapshots in Figure 9.

4 Conclusion and open problems

In this paper, we have proposed and studied a new multi-symplectic numerical integrators for wave map equations on the sphere. This numerical scheme is explicit, conserves the

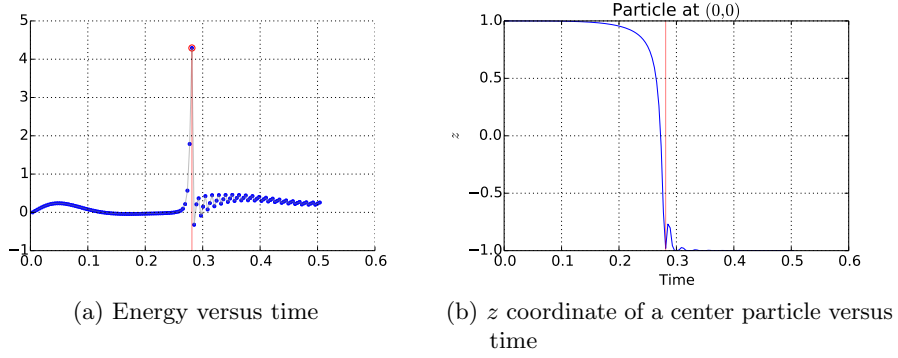


Figure 7: Blow-up of smooth initial data (20).

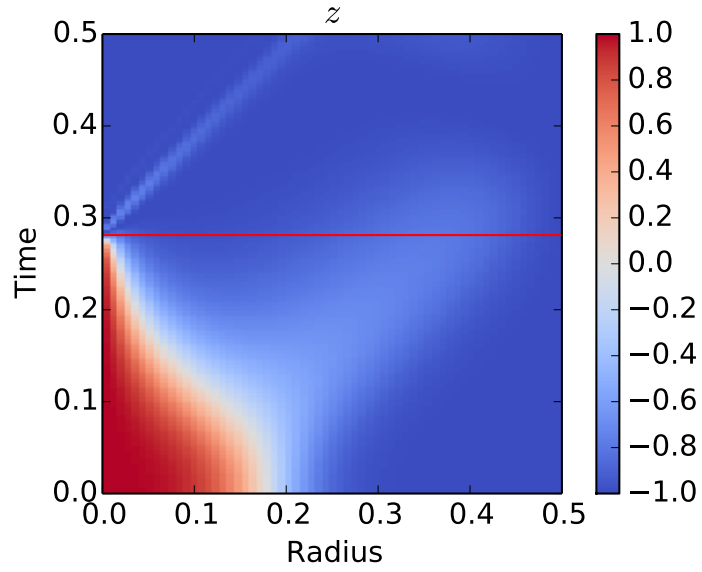


Figure 8: Blow-up: View of the z coordinate versus a radius. The blow-up time is represented by a red line.

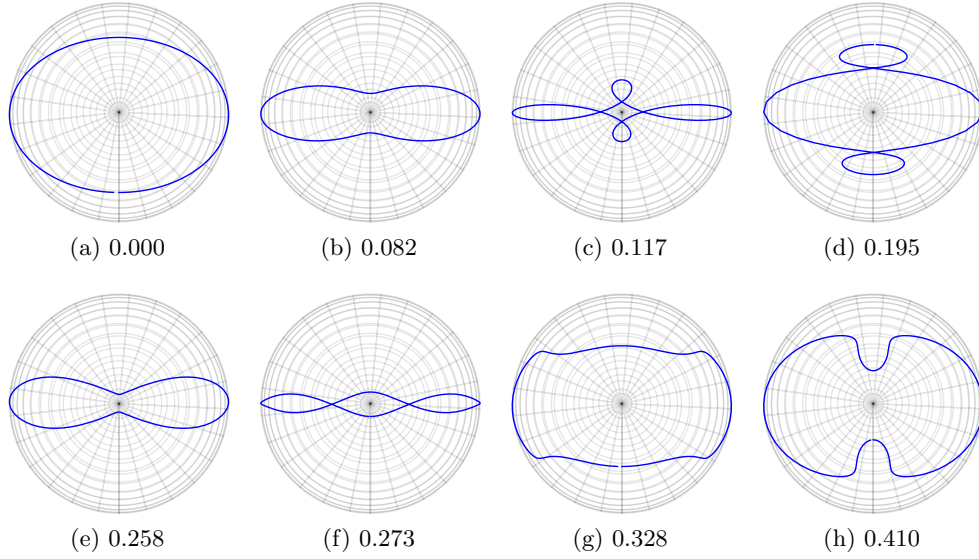


Figure 9: Wave map with potential: Snapshots of the wave map equation with the potential (21). The caption below each snapshot is the time.

constraint, has good conservation properties and can be seen as a generalisation of the SHAKE algorithm for constrained mechanical systems. Furthermore, a convergence of order 2 is observed for smooth solutions.

So far, our numerical study confines to wave map equations on the sphere. However, our method directly allows other target manifolds which are submanifolds of \mathbb{R}^n . Such examples include classical Lie groups and symmetric spaces, see for instance [33]. Furthermore, it would also be interesting to understand whether different splitting of the multi-symplectic matrices could have some effect on the numerical discretisation. In addition, it remains to develop, to try out and further analyse other classical multi-symplectic schemes such as the Preissman box scheme or some multi-symplectic Runge–Kutta collocation methods.

For all these reasons, it seems to us that it would be of interest to get more insight into the behaviour of multi-symplectic schemes for Hamiltonian PDEs with constraints as derived in this publication.

Acknowledgements

DC acknowledges support from UMIT Research Lab at Umeå University. OV acknowledges support from the J.C. Kempe memorial fund (grant no. SMK-1238).

References

- [1] Ľ. Bañas, A. Prohl, and R. Schätzle. Finite element approximations of harmonic

- map heat flows and wave maps into spheres of nonconstant radii. *Numer. Math.*, 115(3):395–432, 2010.
- [2] S. Bartels. Semi-implicit approximation of wave maps into smooth or convex surfaces. *SIAM J. Numer. Anal.*, 47(5):3486–3506, 2009.
 - [3] S. Bartels, X. Feng, and A. Prohl. Finite element approximations of wave maps into spheres. *SIAM J. Numer. Anal.*, 46(1):61–87, 2007/08.
 - [4] S. Bartels, Ch. Lubich, and A. Prohl. Convergent discretization of heat and wave map flows to spheres using approximate discrete Lagrange multipliers. *Math. Comp.*, 78(267):1269–1292, 2009.
 - [5] B. K. Berger, P. T. Chruściel, and V. Moncrief. On “asymptotically flat” space-times with G_2 -invariant Cauchy surfaces. *Ann. Physics*, 237(2):322–354, 1995.
 - [6] P. Bizoń, T. Chmaj, and Z. Tabor. Formation of singularities for equivariant $(2 + 1)$ -dimensional wave maps into the 2-sphere. *Nonlinearity*, 14(5):1041–1053, 2001.
 - [7] J. Bridges, T. Multi-symplectic structures and wave propagation. *Math. Proc. Cambridge Philos. Soc.*, 121(1):147–190, 1997.
 - [8] T. J. Bridges and S. Reich. Multi-symplectic integrators: numerical schemes for Hamiltonian PDEs that conserve symplecticity. *Phys. Lett. A*, 284(4-5):184–193, 2001.
 - [9] J. Frauendiener and R. Peter. Blow-up of the nonequivariant $(2 + 1)$ -dimensional wave map. *ANZIAM J.*, 55(2):151–161, 2013.
 - [10] V. Georgiev and A. Ivanov. Concentration of local energy for two-dimensional wave maps. *Rend. Istit. Mat. Univ. Trieste*, 35(1-2):195–235 (2004), 2003.
 - [11] M. J. Gotay. A multisymplectic framework for classical field theory and the calculus of variations. I. Covariant Hamiltonian formalism. In *Mechanics, analysis and geometry: 200 years after Lagrange*, North-Holland Delta Ser., pages 203–235. North-Holland, Amsterdam, 1991.
 - [12] E. Hairer, C. Lubich, and G. Wanner. *Geometric Numerical Integration*, volume 31. Springer-Verlag, second edition, 2006. Structure-preserving algorithms for ordinary differential equations.
 - [13] J. Isenberg and S. L. Liebling. Singularity formation in $2 + 1$ wave maps. *J. Math. Phys.*, 43(1):678–683, 2002.
 - [14] Trygve K. Karper and Franziska Weber. A new angular momentum method for computing wave maps into spheres. *SIAM J. Numer. Anal.*, 52(4):2073–2091, 2014.

- [15] M. Keel and T. Tao. Local and global well-posedness of wave maps on \mathbf{R}^{1+1} for rough data. *Internat. Math. Res. Notices*, (21):1117–1156, 1998.
- [16] J. Krieger. Global regularity and singularity development for wave maps. In *Surveys in differential geometry. Vol. XII. Geometric flows*, volume 12 of *Surv. Differ. Geom.*, pages 167–201. Int. Press, Somerville, MA, 2008.
- [17] B. Leimkuhler and S. Reich. *Simulating Hamiltonian dynamics*, volume 14 of *Cambridge Monographs on Applied and Computational Mathematics*. Cambridge University Press, Cambridge, 2004.
- [18] J. E. Marsden, G. W. Patrick, and S. Shkoller. Multisymplectic geometry, variational integrators, and nonlinear PDEs. *Comm. Math. Phys.*, 199(2):351–395, 1998.
- [19] R. I. McLachlan, K. Modin, O. Verdier, and M. Wilkins. Geometric generalisations of shake and rattle. *Foundations of Computational Mathematics*, 14(2):339–370, 2014.
- [20] B. Moore and S. Reich. Backward error analysis for multi-symplectic integration methods. *Numer. Math.*, 95(4):625–652, 2003.
- [21] R. Peter and J. Frauendiener. Free versus constrained evolution of the $2 + 1$ equivariant wave map. *J. Phys. A*, 45(5):055201, 19, 2012.
- [22] K. Pohlmeier. Integrable Hamiltonian systems and interactions through quadratic constraints. *Comm. Math. Phys.*, 46(3):207–221, 1976.
- [23] H. Ringström. On a wave map equation arising in general relativity. *Comm. Pure Appl. Math.*, 57(5):657–703, 2004.
- [24] J. Shatah and W. Strauss. Breathers as homoclinic geometric wave maps. *Phys. D*, 99(2-3):113–133, 1996.
- [25] J. Shatah and M. Struwe. *Geometric wave equations*, volume 2 of *Courant Lecture Notes in Mathematics*. New York University, Courant Institute of Mathematical Sciences, New York; American Mathematical Society, Providence, RI, 1998.
- [26] J. Shatah and M. Struwe. The Cauchy problem for wave maps. *Int. Math. Res. Not.*, (11):555–571, 2002.
- [27] J. Shatah and C. Zeng. Constrained wave equations and wave maps. *Comm. Math. Phys.*, 239(3):383–404, 2003.
- [28] M. Struwe. Wave maps. In *Nonlinear partial differential equations in geometry and physics (Knoxville, TN, 1995)*, volume 29, pages 113–153. Birkhäuser, Basel, 1997.
- [29] T. Tao. Ill-posedness for one-dimensional wave maps at the critical regularity. *Amer. J. Math.*, 122(3):451–463, 2000.

- [30] T. Tao. Global regularity of wave maps. ii. small energy in two dimensions. *Comm. Math. Phys.*, 224(2):443–544, 2001.
- [31] D. Tataru. The wave maps equation. *Bull. Amer. Math. Soc. (N.S.)*, 41(2):185–204 (electronic), 2004.
- [32] D. Tataru. Rough solutions for the wave maps equation. *Amer. J. Math.*, 127(2):293–377, 2005.
- [33] C.-L. Terng and K. Uhlenbeck. $1 + 1$ wave maps into symmetric spaces. *Comm. Anal. Geom.*, 12(1-2):345–388, 2004.
- [34] J. Zhai, J. Fang, and L. Li. Wave map with potential and hypersurface flow. *Discrete Contin. Dyn. Syst.*, (suppl.):940–946, 2005.